CHEMISTRY OF MATERIALS

pubs.acs.org/cm

Article

Synthesis and Characterization of $(FA)_3(HEA)_2Pb_3I_{11}$: A Rare Example of <1 1 0>-Oriented Multilayered Halide Perovskites

Maroua Ben Haj Salah, Nicolas Mercier,* Magali Allain, Antonin Leblanc, Jens Dittmer, Chiara Botta, Claudio Quarti, and Claudine Katan*

Cite This: https://doi.org/10.1021/acs.chemmater.2c00130

Read Online

ACCESS | Metrics & More | Article Recommendations | Supporting Information

ABSTRACT: Metal-halide perovskites have recently demonstrated great potential for a wide variety of optoelectronic applications, with their layered subfamily offering improved stability as compared to their three-dimensional analogues. Among the layered compounds, a subclass of <1 0 0> terminated compounds are currently dominating the field, while the <1 1 0> subclass is comparably much less explored. Here, we report on the synthesis of $(FA)_3(HEA)_2Pb_3I_{11}$ obtained by room-temperature liquid−gas diffusion involving the intermediate-size cation hydroxyethylammonium (HEA^+), formamidinium (FA^+), and PbI_2 dissolved in an acidic solution. This multilayered hybrid perovskite is a rare example of a m = 3 member of the <1 1 0>-oriented series $(A')_2(A)_mB_mX_{3m+2}$. Structural characterization based on X-ray diffraction and nuclear magnetic resonance investigations reveals that the small-size cation FA^+ is located both in the inner layer of the perovskite sheet and in the interlayer space, while the intermediate-size cation HEA^+ is situated in the outer cavities of the perovskite sheet. $(FA)_3(HEA)_2Pb_3I_{11}$ exhibits a broad absorption band in the visible region (400−650 nm) leading to an optical band gap of 1.96 eV. Electronic structure calculations confirm the direct nature of the band gap and evidence sizable interlayer electronic coupling related to short I...I distances. These features are reminiscent of those observed for <1 0 0>-oriented Pb_3I_{10} analogues that have shown photovoltaic efficiencies over 18%. These findings should prompt further investigations for the design of other <1 1 0>-oriented multilayered (m = 3, 4,...) metal-halide perovskites.

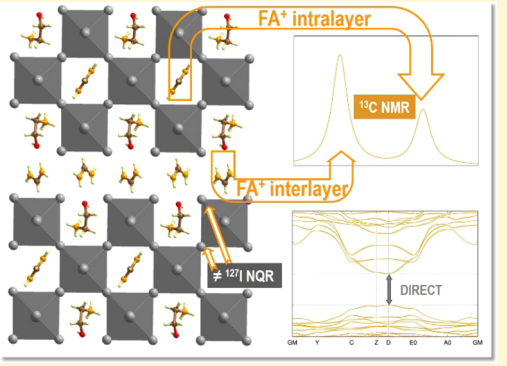

INTRODUCTION

Layered halide perovskites that have attracted much attention in the 1990s and the beginning of the 2000s,[1−11] most effort being focused on chemistry, structural, and optical characterizations, have also revealed in recent years great potential for various applications including photovoltaics.[12−19] Since the discovery of a photovoltaic effect using the three-dimensional (3D) metal-halide perovskite $(CH_3NH_3)PbI_3$ as an absorber in 2009,[20] 3D organic−inorganic materials have attracted wide attention for photovoltaic applications (PSC technology).[21−24] However, the limited stability of 3D perovskite materials and their degradation under operative conditions imposed a critical limit for the exploitation of these materials.[25−27] This remotivated the interest for layered systems that, thanks to the incorporation of bulky hydrophobic organic cations, present much improved stability compared to their 3D counterpart.[12−15] Since the 1990s, layered perovskites have also been known to exhibit photoluminescence (PL) properties with narrow emission, whose energy depends on the nature of the halides,[1,9] while electroluminescence was demonstrated at low temperature.[8] More recently, it has been discovered that some lead-halide layered perovskites display broad band emission (white emission),[28−31] while electroluminescence at room temperature with high quantum efficiencies was demonstrated, particularly for 2D/3D systems[32−34] (mixtures of layered and 3D perovskites).

Two main families of low-dimensional perovskites are known, called <1 0 0>- and <1 1 0>-oriented layered perovskites, as proposed by Mitzi.[1] The different perovskite networks of each of this family can be obtained by cutting the ABX_3 (A^+ is a small cation, B is metal, and X is halogen) mother structure along the (1 0 0) and (1 1 0) reticular planes every n or m layers, leading to B_nX_{3n+1} and B_mX_{3m+2} anionic frameworks for the <1 0 0>- (n series) and <1 1 0>-oriented (m series) layered perovskites, respectively. By far, the most common layered compounds (butylammonium and phenylethylammonium lead-halide perovskites at the forefront) belong to the <1 0 0>-oriented family.[35] Their general formula is $(A')_2(A)_{n-1}B_nX_{3n+1}$ or $(A'')(A)_{n-1}B_nX_{3n+1}$ (A'^+ and A''^{2+} are

Received: January 17, 2022
Revised: June 14, 2022

cations in the interlayer space). If most of the known perovskites belonging to this family have a single layer (n = 1) of corner-sharing octahedra sandwiched between templating cations, more and more multilayered materials (n > 1) have been recently reported because of their potentialities in PSCs.[36,37] The general formula of corrugated <1 1 0>-oriented compounds instead is either $(A')_2(A)_mB_mX_{3m+2}$, $(A)_{m+2}B_mX_{3m+2}$, or $(A'')_2(A)_{m-2}B_mX_{3m+2}$. For the two last categories, mostly m = 2 type compounds are known: $(A)_4B_2X_8$ (A^+ = guanidinium, B = Pb, Sn, X = I;[38,39] A^+ = acetamidinium, B = Pb, X = Br)[40] and several $(A'')_2B_2X_8$ materials.[28,29,41−47] This last type of perovskite became famous because (EDBE)$PbBr_4$ (≈$(EDBE)_2Pb_2Br_8$ (m = 2), $EDBE^{2+}$ = 2,2′-(ethylendioxy)bis(ethylammonium)) was one of the first halide perovskites exhibiting broad band emission,[29] which leads to the emerging domain of halide perovskites for white light emission application.[16,30] Until now, the only series of such multilayered perovskites has been reported by Mitzi for the iodoformamidinium/methylammonium/Sn^{2+}/I^- system: $(NH_2C(I)=NH_2)_2(CH_3NH_3)_mSn_mI_{3m+2}$ (m = 2−4).[3] The electrical properties of these halide perovskites are compared to that of <1 0 0>-oriented perovskites (n series) $(C_4H_9NH_3)_2(CH_3NH_3)_{n-1}Sn_nI_{3n+1}$ (n = 1−5),[2] revealing "a consistent exponential drop in low temperature resistivity with increasing perovskite layer thickness, and approximately independent of layer orientation." This highlights the potentiality of such rarer <1 1 0>-oriented multilayered perovskites (m = 3, 4,...) in all fields already covered by the <1 0 0>-oriented perovskites, including photovoltaics. Moreover, only crystal structures for m = 2 perovskites, including $(NH_2C(I)=NH_2)_2(CH_3NH_3)_2Sn_2I_8$,[3] have been reported until now.

We report here the synthesis and, to the best of our knowledge, the first successful XRD structural characterization of m = 3 <1 1 0>-oriented hybrid perovskites, in the form of $(FA)_3(HEA)_2Pb_3I_{11}$ perovskite (FA^+: formamidinium, HEA^+: hydroxyethylammonium). Structural investigation is complemented by solid-state nuclear magnetic resonance (NMR) measurements and first-principles calculations. The simulations are further used to highlight the potential of nuclear quadrupole resonance (NQR) spectroscopy to provide information on the local structure. We show that the small-size cation FA^+ is located both within perovskite sheets (cubic site) and in the interlayer space. The HEA^+ cation is found in the outer cavities, playing a templating role and leading to the formation of the specific <1 1 0>-oriented perovskite network. The optical and electronic properties are studied via optical spectroscopy (absorption and PL) and periodic density functional theory (DFT) simulations, respectively. The material shows an absorption onset at 1.96 eV, and the computed band structure has a direct character. Furthermore, the short distance between consecutive inorganic perovskite sheets is shown to result in effective masses close to m_e (that is, comparable to promising organic molecular semiconductors), suggesting improved out-of-plane charge and energy transport as compared to the well-known alkylammonium (butylammonium and hexylammonium) based <1 0 0>-oriented layered lead-iodide perovskites. These characteristics are comparable to those of (4AMP)$(MA)_2Pb_3I_{10}$ that has recently been demonstrated to achieve a solar cell efficiency of 18,3%, boosted by light-induced interlayer contraction.[48] The present work suggests that similar potential exists for the <1 1 0>-oriented family.

EXPERIMENTAL SECTION

Synthesis and Characterization. The $(FA)_3(HEA)_2Pb_3I_{11}$ material has been prepared as a pure phase, in great quantity and high yield, by room-temperature solution techniques. Iodide salts (PbI_2, FAI, and HEAI) were first dissolved in a hydriodic acid solution (see the SI for details). The resulting saturated solution was placed into a sutured ethyl acetate vapor atmosphere leading through a liquid−gas diffusion process to crystals of $(FA)_3(HEA)_2Pb_3I_{11}$ after 1 day. The dark red plate-like crystals were filtered off (Figure S1), washed several times with ethyl acetate, and dried at 40 °C for 30 min. X-ray powder diffraction analysis which was performed on a D8 Bruker diffractometer (Cu Kα) equipped with a linear Vantec super speed detector confirmed the phase purity of the title compound, showing that all observed reflections could be indexed in the unit cell obtained from single-crystal X-ray diffraction experiments (Figure S2). Chemical analysis (C, O, N, H) carried out on a crystallized sample of $(FA)_3(HEA)_2Pb_3I_{11}$ confirmed the expected formula (calculated (wt%): C, 3.68; H, 1.36; N, 4.92; O, 1.40. Experimental: C, 3.66; H, 1.29; N, 4.90; O, 1.37). Moreover, ^1H solution NMR of crystallized powder solubilized in [D_6] DMSO (SI, Figure S3) allowed us to determine the FA^+/HEA^+ ratio of 1.51, which is in good agreement with the expected formula of $(FA)_3(HEA)_2Pb_3I_{11}$. Thermogravimetric analysis (TGA) shows that $(FA)_3(HEA)_2Pb_3I_{11}$ is stable up to 200 °C while no signature of phase transition in the RT-200 °C range is detected by means of differential scanning calorimetry (DSC) analysis (Figure S4).

Single-Crystal X-Ray Crystallography. X-ray diffraction data were collected at T = 280.0(1) K, on a Rigaku Oxford Diffraction diffractometer equipped with an Atlas CCD detector and microfocus Cu-K_α radiation (λ = 1.54184 Å). Intensities were corrected for Lorentz-polarization effects, as well as for absorption effect (gaussian method using CrysAlisPro program-CrysAlisPro, Rigaku Oxford Diffraction, V1.171.40.45a, 2019). The structures were solved using the SHELXT program and refined by full matrix least-squares routines against F^2 using SHELX programs (G. M. Sheldrick 2018, SHELXT 2018/2 and SHELXL 2018/3). The hydrogen atoms were treated with a riding model except for the H atom on the hydroxyl group which were first placed at the calculated position taking into account the local electron density and then fixed with the HFIX constraint for the convergence of the refinement. The refinements of positions and anisotropic thermal motion parameters of the non-H atoms converge to $R_{(F)}$ = 0.0532 (3069 independent reflections (R_{int} = 0.0378), 142 parameters), $wR2_{(F2)}$ = 0.1443 (all data), and GOF on F^2 is 1.052. Many restraints on the distances and angles of the three organic molecules were applied to be in agreement with the geometry of such molecules. This suggests possible dynamic disorder of the organic cations. A summary of crystallographic data and refinement results is listed in Tables S1 and S2. A complete list of crystallographic data, along with the atomic coordinates, the anisotropic displacement parameters, and bond distances and angles is given as a CIF file. CCDC number 2098405.

Electronic Band Structure Calculations. Electronic properties of the material are investigated for the newly reported crystal structure of $(FA)_3(HEA)_2Pb_3I_{11}$, assumed as a pure phase. We adopted periodic DFT calculations, within the plane-wave/pseudopotential formalism, as implemented in the pwscf program from the Quantum Espresso suite software.[49] We adopted norm-conserving pseudopotentials, as available from the pseudodojo data set,[50] and set kinetic energy cutoff to 50 Ry and 200 Ry for the plane-wave expansion of the electron wavefunction and electron density, which provides accurate results for lead-iodide perovskite networks.[51] Electronic structures are based on the PBE exchange-correlation functional,[52] with spin-orbit-coupling explicitly accounted.[53] A homogeneous 4 × 6 × 2 sampling of the first Brillouin zone in the Monkhorst Pack scheme[54] with different sampling reflects the anisotropy in the lattice parameters (shorter parameters are associated with denser k-point sampling). In light of the presence of a molecular component, we addressed the potential impact of van der Waals interactions. Namely, we performed partial optimization of the organic component both

https://doi.org/10.1021/acs.chemmater.2c00130
Chem. Mater. XXXX, XXX, XXX−XXX

adopting DFT-D2 semiempirical corrections[55] and a fully ab initio VDW-DF2 functional[56] for the description of the exchange and correlation. Corresponding band structures are reported in the Supporting Information (Figures S12 and S13) and clearly point out toward a very limited role of the van der Waals interactions in affecting the electronic structure of the material.

First-Principles Prediction of Solid-State NMR and NQR Signals. This is based on periodic, plane-wave/pseudopotential DFT simulations, as implemented in the CASTEP suite code.[57] This code adopts a perturbative approach to evaluate the chemical shielding tensor of the atoms composing the investigated crystal model. The present method also takes advantage of the GIPAW (Gauge Including Projector Augmented Wave) formalism to map back the nonlocal information from the plane-wave basis set to the local information associated with the electron shielding close to the nuclei, meanwhile solving the Gauge problem, typical of finiteness of the basis set.[58,59] A kinetic energy cutoff of 500 eV and 0.03 $Å^{-1}$ automatic sampling of the first Brillouin zone have been employed, as best trade-off between accuracy and computational cost.[60] Although crucial for a proper description of the NMR signals of ^{207}Pb nuclei,[61] the present calculations do not include spin-orbit-coupling, as this is not currently available in CASTEP. The same computational formalism and details are adopted for the estimate of the Electric Field Gradients and corresponding NQR parameters (namely, quadrupolar coupling constants, C_q, and asymmetry parameters, η).

Experimental Solid-State NMR. Solid-state NMR spectra have been acquired on a Bruker Avance III 300 MHz WB spectrometer equipped with a 4 mm X/H MAS probe used for ^{13}C and a 1.3 mm X/H MAS probe used for ^{207}Pb. ^{13}C direct excitation experiments were performed under 5 kHz MAS by means of the DEPTH sequence for background suppression and with proton decoupling; 1 K scans were accumulated with a recycle delay of 40 s. ^{207}Pb experiments were performed with a spinning frequency of 40 kHz. The ARING sequence was used for background suppression; 500 K scans were accumulated with a recycling delay of 240 ms.

Optical Properties. Optical absorption is performed with a UV−Vis Lambda9 spectrometer. PL and PLE spectra are obtained with a NanoLog composed of a iH320 spectrograph equipped with a Synapse QExtra charge-coupled device and a PPD-850 single photon detector by exciting with a monochromated 450 W Xe lamp. The spectra are corrected for the instrument response. Time-resolved TCSPC measurements are performed with a PPD-850 single photon detector module and a DeltaTime series DD-405 L DeltaDiode Laser. Analysis of the emission decays is performed with the instrument Software DAS6. The average emission lifetime is obtained as $\tau = \sum A_i t_i$ by multiexponential fits of the decays $I = \sum A_i \exp(t/t_i)$.

RESULTS AND DISCUSSION

Structural Aspects. In the $HEA^+/Pb^{2+}/I^-$ system, the <1 0 0>-oriented layered perovskite $(HEA)_2PbI_4$ (n = 1) has been obtained by our group in a previous study.[10] An interesting structural feature was the unique hydrogen-bond network connecting adjacent layers owing to OH...I, NH_3^+...I_{apical}, and intermolecular NH_3^+...OH interactions. In contrast, only weak NH_3^+...$I_{equatorial}$ hydrogen interactions were counted. As a result, a significant reduction of the band gap was correlated with weak distortions of perovskite layers. More recently, working with the MA^+ or $FA^+/HEA^+/Pb^{2+}/I^-$ system in order to prepare multilayered Ruddlesden−Popper phases, we discovered a new family of 3D materials, called lead-deficient hybrid perovskites (d-HP) $(HEA,A)_{1+x}Pb_{1-x}I_{3-x}$ (A: MA^+, FA^+). The single-crystal X-ray study led to solve the inorganic 3D network but, unfortunately, organic cations were not localized.[62,63] In the present work, the same reagents exposed to different experimental conditions brought a pure phase of the <1 1 0>-oriented multilayered m = 3 perovskite $(FA)_3(HEA)_2Pb_3I_{11}$ in the form of plate-like crystals.

The crystal structure was solved in the P2 monoclinic space group (see general view, Figure 1a, Tables S1 and S2). Let us

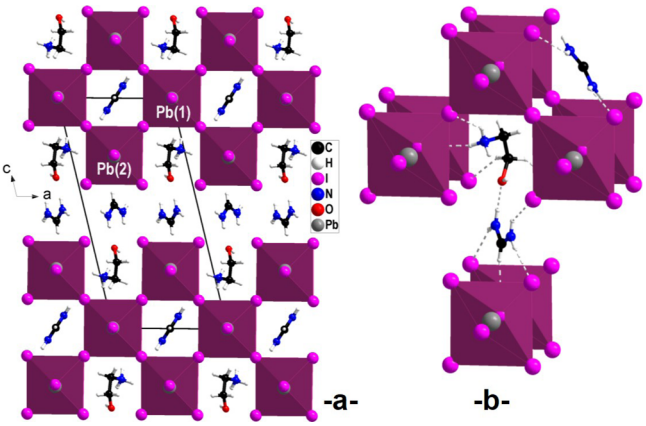

Figure 1. Structure of the <1 1 0>-oriented hybrid perovskite $(FA)_3(HEA)_2Pb_3I_{11}$: General view along the b direction (a) and partial view showing FA^+ cations localized both in the inner cavity of the perovskite sheet and in the interlayer space and HEA^+ cations localized in outer perovskite cavities (b) (dashed lines: H...I and H...O contacts <3.10 Å).

notice that the inorganic framework can be correctly described either in a twice greater orthorhombic unit cell or in a corresponding centrosymmetrical monoclinic space group. However, organic components could be correctly located only within the $P2$ space group, and considering constraints on bond lengths and angles (see the Experimental Section). An interesting structural feature is that a nearly undistorted perovskite sheet is obtained (Figure 1a). The inner $Pb(1)I_6$ octahedra exhibit six similar Pb−I bond lengths (3.18−3.20 Å range), whereas for the outer $Pb(2)I_6$ octahedra, the Pb−$I_{terminal}$ bond lengths appear only slightly shorter (3.093 Å) than the Pb−I ones involving shared iodides (3.167−3.303 Å range). As regards bond angles, the I−Pb−I ones are close to 90° (adjacent iodides) or 180 ° (opposite iodides), and more importantly, the Pb−I−Pb ones, revealing the degree of distortion of perovskite layers, are almost linear (177.7°). As underlined in a recent review,[17] <1 1 0>-oriented multilayered perovskites with m = 2 very often exhibit highly distorted inorganic networks, especially those based on dications (A''^{2+}) linking two adjacent sheets. Here, the combined effect of HEA^+ located in outer cavities and FA^+ placed in the interlayer space leads to these unusual undistorted perovskite sheets. The HEA^+ cation, which has also afforded the m = 2 hybrid perovskite in the lead/bromide system,[45] has surely a templating role in the formation of such a network due to its ability both to fill the rectangle parallelepiped space and to interact with iodides through H...I bonding and with FA^+ cations located in the interlayer space through NH_2...OH bonding (Figure 1b). FA^+ cations are therefore localized both in the inner layer of the perovskite sheet (cubic site) and in the interlayer space, so that a formula of $(FA)_2[(HEA)_2(FA)Pb_3I_{11}]$ is better suited to account for the specific structural arrangement.

Another structural feature observed in such <1 1 0>-oriented perovskites is short I...I interlayer distances. In $(FA)_3(HEA)_2Pb_3I_{11}$, the I...I contact is roughly twice the van der Waals radii (d(I...I) = 4.547 Å). This interlayer distance is much smaller than the one of known <1 0 0>-oriented

https://doi.org/10.1021/acs.chemmater.2c00130
Chem. Mater. XXXX, XXX, XXX−XXX

structures adopting a staggered interlayer arrangement with shifts of half a crystal unit cell in the two in-plane directions, also named Ruddlesden−Popper phases. While remaining slightly larger than those of the eclipsed $(4AMP)(MA)_2Pb_3I_{10}$ compound,[64] so called Dion−Jacobson phase, it is comparable to that of $(GA)(MA)_3Pb_3I_{10}$ that shows a similar pattern with the layer shifted by half a unit cell vector only in one of the in-plane directions.[65]

The presence of FA^+ in a cubic site of a iodoplumbate perovskite at room temperature is quite unusual. In fact, as is well known, the 3D α-$FAPbI_3$ compound is stable above 150 °C at ambient pressure, while the room-temperature stable phase is the δ-$FAPbI_3$ (yellow color) having 1D inorganic PbI_3^- chains of face-sharing octahedra.[66] Layered iodoplumbate perovskites (n series) including FA^+ are also rare, even if organic dications in the interlayer space have successfully stabilized such layered perovskites (n = 2,...).[67]

Given these observations, we performed investigations to assess the stability of $(FA)_3(HEA)_2Pb_3I_{11}$. When kept in an inert atmosphere at room temperature (RT), $(FA)_3(HEA)_2Pb_3I_{11}$ is stable (Figure S5a). In addition, TGA and DSC experiments (Figure S4) reveal no thermal accident in the RT-150 °C temperature range before the decomposition occurs. However, it appears that this compound is unstable under physical strain or in a humid atmosphere at RT, leading to a decomposition into δ-$(FA)PbI_3$ and certainly into $(FA)_2(HEA)_2Pb_2I_8$, the m = 2 member of the $(FA)_m(HEA)_2Pb_mI_{3m+2}$ series (<1 1 0> series). This is clear from PXRD analysis of samples previously ground one to 2 min in an inert atmosphere, or under exposure in an air atmosphere (humidity rate of ≈40%), with decreasing intensity of the X-ray lines associated with $(FA)_3(HEA)_2Pb_3I_{11}$ together with the appearance of specific X-ray lines of both δ-$(FA)PbI_3$ and $(FA)_2(HEA)_2Pb_2I_8$ (Figures S5b and S6). Notice that the synthesis and crystal structure determination of this last compound (Figure S7 and Table S3) allowed us to get its corresponding calculated PXRD pattern. Overall, the novel $(FA)_3(HEA)_2Pb_3I_{11}$ shows improved stability to moisture, as compared to reference $MAPbI_3$ 3D halide perovskite. The latter in fact degrades in PbI_2 already within 24 h under a humidity rate of 40%, while the m = 3 compound does not evidence signatures of m = 2 layered phase and/or α-FAPI for 1 week under the same conditions (Figure S5).

^{13}C NMR was used to obtain further structural information, especially related to the location of the organic cations. While ^{13}C NMR is usually performed as cross-polarization (CP), this technique is less suited for hybrid perovskites, as the organic cations can be very mobile in terms of reorientations, partly averaging out the necessary dipolar coupling.[68,69] The relatively narrow width of the ^1H signals shows that the cations are indeed mobile, which is furthermore an indication of good and regular insertion (Figure S10). Therefore, the experiments have been performed by direct excitation, which is moreover quantitative. There are three different cation sites, that is, interlayer, inner layer, and outer cavity (Figure 1). The ^{13}C spectrum (Figure 2a) shows the two HEA signals at 61.8 (...−$\underline{CH_2}$−OH) and 45.8 (...−$\underline{CH_2}$−NH_3^+) ppm with only minor dispersion (in the form of a small signal feet), indicating that they overall occupy one of the three potential sites, consistent with the particular role attributed to the HEA^+ cations on the outer cavity of the perovskite layers (vide infra). Periodic DFT calculations of the chemical shielding tensor performed on the model in Figure 1, where HEA^+ cations are placed in the outer cavities, yield to chemical shifts for ^{13}C nuclei of HEA^+ within few ppm with respect to the experimental data (see Figure 2), namely at 65.2 ppm (...−$\underline{CH_2}$−OH) and 44.7 ppm (...−$\underline{CH_2}$−NH_3^+). These computed chemical shifts and the existence of only one signal per carbon also indicate that HEA^+ cations are likely to seat in the outer cavities of the inorganic sheet. In contrast, the formamidinium cation shows a group of three signals. This might on the first glance indicate an occupation of all three possible sites; however, one of them turns out to be an experimental artifact. The central signal at 156.3 ppm corresponds to the nonperovskite δ-phase of formamidinium-PbI_3 (FAPI), product of degradation upon physical strain to which this material is sensitive as revealed by a DRX pattern of a ground sample (vide supra and Figure S6).[70] In fact, also previous NMR studies in the literature pointed toward material degradation due to the measuring procedure itself.[71−73] Degradation therefore turns out to be inevitable when performing NMR, even with very careful filling of the NMR rotor, as the magic angle spinning with at least 3 kHz necessary for spectral

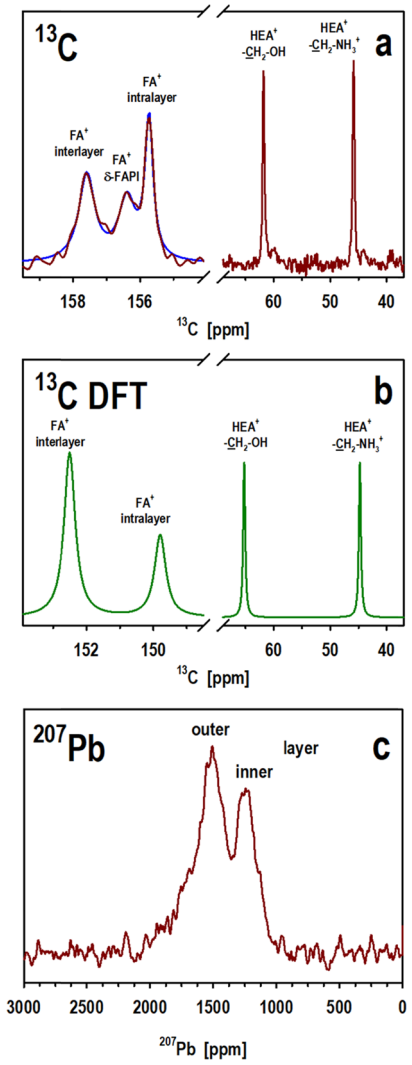

Figure 2. (a) Direct excitation ^{13}C spectrum of $(FA)_3(HEA)_2Pb_3I_{11}$ (red) and deconvolution of the FA^+ signal group with three lorentzians (blue). (b) Simulated ^{13}C spectrum based on the chemical shieldings extracted from a DFT-calculated electronic structure. (c) ^{207}Pb spectrum.

https://doi.org/10.1021/acs.chemmater.2c00130
Chem. Mater. XXXX, XXX, XXX−XXX

resolution applies much physical strain to at least a part of the sample powder. XRD of the material after MAS NMR confirms the formation of this phase in previously pure samples (data not shown). Humidity enhances the effect: Figure S8a shows the formamidinium ^{13}C NMR region of a less (sample 1) and very (sample 2) carefully stored and prepared sample, and a sample deliberately degraded by keeping it in 100% humidity, compared to a sample of FAPI mainly in the δ-phase. The center signal is increasing, representing already 75% in sample 1, and corresponds to δ-FAPI. On the side of HEA^+, a progressed degradation (sample 2) is not manifested by additional distinct signals, but line broadening and dispersion around the initial m = 3 signals (Figure S8b), in particular for ...−$\underline{CH_2}$−OH (65.2 ppm). This is consistent with the proposed formation of m = 2 structures, in which the HEA^+ cations have essentially the same local environment (Figure S7). The effect is better visible by CP experiments in which the carbons in less perfect structures are enhanced, as there are more constraints to cation reorientational motions.[63] In the deliberately humidity degraded sample, the HEA^+ ions are already in a sort of solution state, as seen from the strong shift, very narrow signals (experimentally limited by the acquisition time) and the absence of signals in the CP spectrum.

There are thus two distinct FA signals of the $(FA)_3(HEA)_2Pb_3I_{11}$ phase itself, at 157.6 and 155.6 ppm, with an intensity ratio of 0.55:0.45. This matches, within the experimental uncertainty, the picture of formamidinium occupying the interlayer site and the inner perovskite intralayer site with a stoichiometric ratio of 2:1 (Figure 1). This assignment is further confirmed by DFT calculations (Figure 2b), which predict ^{13}C at 152.5 and 149.8 ppm for the two FA^+ cations in the interlayer cavity and the one in the intralayer cavity, respectively. Similarly to HEA^+, the computed absolute values are shifted with respect to the experimental ones, but the distance between the two signals matches relatively well.

The ^{207}Pb spectrum (Figure 2c) is consistent with the ^{13}C findings: there are two signals of intensity ratio of roughly 1:2, which we therefore tentatively assign to the inner (1240 ppm) and outer (1500 ppm) layer lead atoms. However, both signals do not have a perfect shape, which is probably due to smaller contributions of degradation products as discussed above. While m = 2 is expected to have a similar chemical shift to the outer layer, the 1240 ppm signal probably contains a contribution of the δ-FAPI phase upfield. The latter is illustrated in Figure S9: the $(FA)_3(HEA)_2Pb_3I_{11}$ sample is compared with a δ-FAPI (which still contains a residual δ phase) and the further degraded sample 1 with very high (75%) degree of δ-FAPI formation. Theoretical calculations of the NMR frequencies of ^{207}Pb confirm the experimental data; they predict 838 ppm for the inner and 1038 ppm for the outer layer lead. In addition to the general 400 ppm underestimation, which is often observed in chemical shift calculations, the order is consistent and the difference of 200 ppm between the two signals is not too far from the experimental value of 260 ppm. Previous simulations performed on other mixed halide perovskites provided a similar shift of ^{207}Pb signals compared to the experiment.[60]

The NQR technique was also employed in the past for the structural characterization of halide perovskite materials,[74−80] especially in relation to the local chemical environment probed by the halide, that, presenting nuclear spin I > 1/2, is subject to quadrupolar interaction with the electric field gradient. However, we did not observe any ^{127}I signal for the m = 3 compound likely because of extreme line broadening caused by inherent disorder associated with the organic component, which in particular has been observed for mixed-cation halide perovskites.[79−81] Nevertheless, DFT may provide useful feedback about the expected response of iodine in $(FA)_3(HEA)_2Pb_3I_{11}$, so to extend the overall limited amount of results reported in the literature,[74−80] and narrow the field for future experimental investigation on this or similar compounds. In Table 1, we report the values of the computed

Table 1. DFT Computed NQR Response for ^{127}I Nuclei in the Reference γ-Phase of $CsPbI_3$ Perovskite and in the Investigated M = 3 Layered $(FA)_3(HEA)_2Pb_3I_{11}$ Perovskite[a]

	C_q (MHz)	η	1/2 → 3/2 (MHz)		3/2 → 5/2 (MHz)	
			Theo	Expt[79]	Theo	Expt[79]
γ-$CsPbI_3$						
I_c	543.46	0.02	81.54	77.75	163.03	155.34
I_d	566.19	0.13	86.73	81.50	169.32	160.88
$(FA)_3(HEA)_2Pb_3I_{11}$						
I_{bulk}	591.53	0.03	80.80		177.43	
	534.67	0.03	80.26		160.38	
	535.36	0.02	80.40		160.59	
	559.09	0.04	84.01		167.67	
I_{term}	262.54	0.90	64.97		70.58	
	286.26	0.71	61.97		79.45	

[a] C_q and η are the computed quadrupolar coupling constant and the asymmetry parameter, respectively. Corresponding NQR resonances for the 1/2 → 3/2 and 3/2 → 5/2 transitions are reported as well and compared to experimental results (when available).

quadrupolar interaction constant (C_q), asymmetry parameter (η), and corresponding spin-transition frequencies for the ^{127}I nuclei in two cases of interest, namely, the γ-phase of $CsPbI_3$, taken as reference, and our m = 3 layered halide perovskite. Because ^{127}I has a 5/2 nuclear spin, it presents two times two allowed transitions, ±1/2 → ±3/2 and ± 3/2 → ±5/2. For γ-$CsPbI_3$, our theoretical data nicely match both previous DFT estimates and the experimental data available from the literature,[79] hence supporting the reliability of our methodology. Most notably, DFT calculations predict the presence of two distinct signals, both for the 1/2 → 3/2 (81.54 and 86.73 MHz) and the 3/2 → 5/2 transition (163.03 and 169.32 MHz), in agreement with experiment. The presence of these doublets reflects the different environment experienced by the nonequivalent ^{127}I nuclei in the γ-phase of $CsPbI_3$, which lie at the c (apical; I_c) and d (equatorial; I_d) Wyckoff positions, respectively, of the corresponding *Pnam* space group.[82]

For the $(FA)_3(HEA)_2Pb_3I_{11}$ compound, the situation is more involved, as the poor symmetry evidenced from XRD measurements results in several nonequivalent crystalline sites for the ^{127}I nuclei, each with different NQR features. Still, a chemically driven classification emerges when distinguishing between bulk (I_{bulk}) and terminal iodines (I_{term}), bounded to two and one lead atoms, respectively. The NQR response of bulk iodines in the multilayered $(FA)_3(HEA)_2Pb_3I_{11}$ perovskite is close to that of iodines in the 3D γ-$CsPbI_3$ phase, showing signatures for the 1/2 → 3/2 and 3/2 → 5/2 transitions in the range of 80−84 MHz and 160−180 MHz, respectively. In contrast, terminal iodines present spin-transitions at comparably smaller frequencies, 62−65 MHz and 71−78 MHz for the 1/2 → 3/2 and 3/2 → 5/2, respectively. The smaller splitting between the 1/2 → 3/2 and 3/2 → 5/2 transitions

https://doi.org/10.1021/acs.chemmater.2c00130
Chem. Mater. XXXX, XXX, XXX−XXX

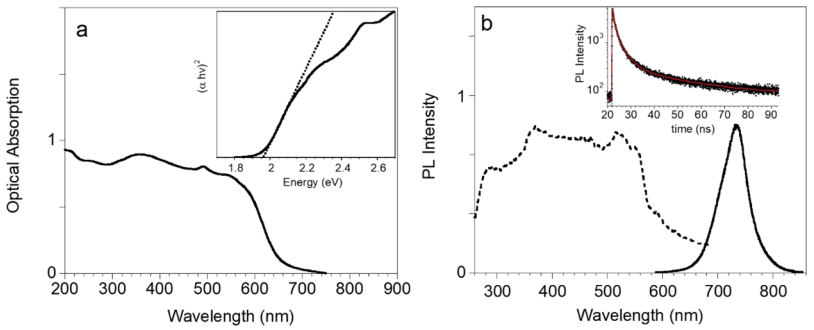

Figure 3. (a) Optical absorption, Tauc Plot (inset), (b) PL (solid line), and PLE spectra (dashed line) of $(FA)_3(HEA)_2Pb_3I_{11}$. Excitation wavelength 540 nm, emission 740 nm. In the inset, the emission decay (solid points) recorded at 740 nm with three-exponential fit (red solid line) is reported. Fitting parameters: (0.2845) 3.707 ns; (0.6694) 0.803 ns; (0.0460) 29.76 ns; χ^2 = 1.31081.

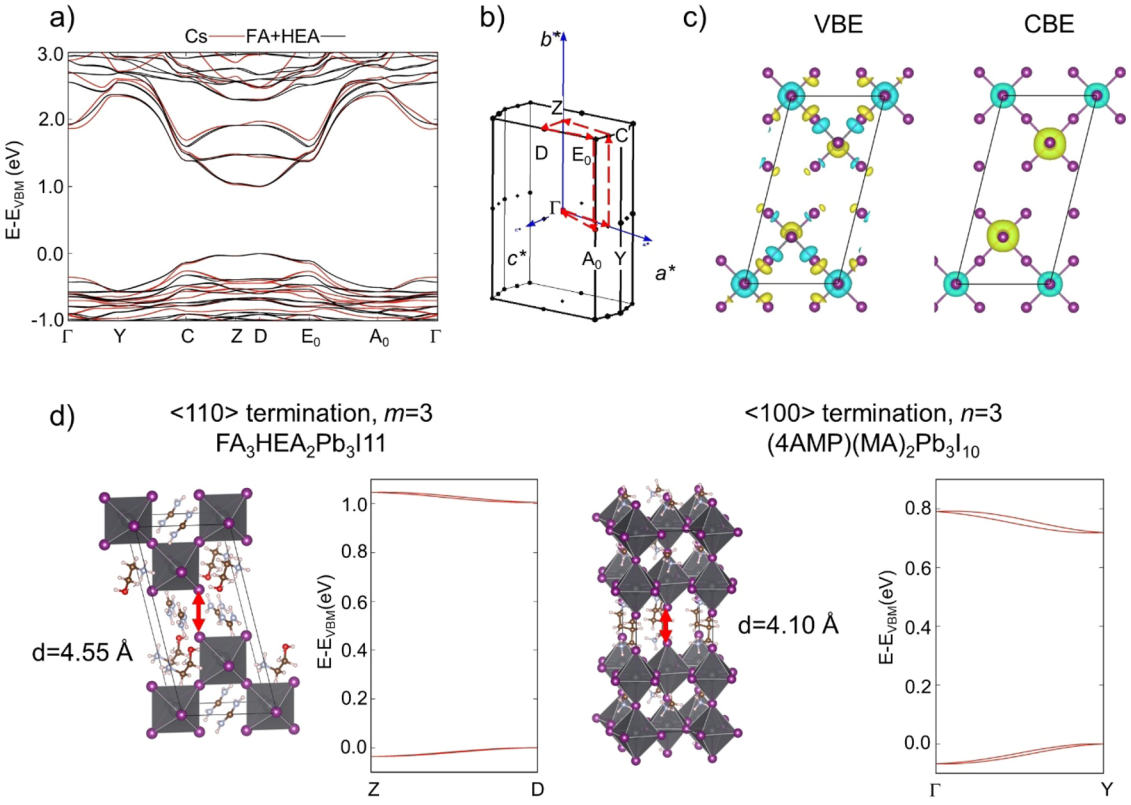

Figure 4. (a) DFT-SOC band structure computed for $(FA)_3(HEA)_2Pb_3I_{11}$ both considering the Cs atoms in place of the FA and HEA (Cs) and considering the organic moieties explicitly (FA + HEA); (b) corresponding first Brillouin zone with high symmetry points; (c) isosurfaces computed for the wave-functions associated with the valence band edge (VBE) and conduction band edge (CBE). The threshold for the isosurface is set to 3×10^{-4} e/bohr;[3] (d) structure and band dispersions along the stacking direction for the currently investigated <1 1 0>-oriented m = 3 layered perovskites and for reference <1 0 0>-oriented n = 3 layered perovskites. The latter structure is taken from ref 64.

compared to bulk iodines is related to the very large asymmetry parameter η for terminal iodines. All findings clearly confirm the undeniable sensitivity of the NQR technique in probing the perovskite local structure[74−80] and shall raise further attempts in this direction, especially whenever less disorder is present.

Optical Absorption and Photoluminescence. The optical absorption of $(FA)_3(HEA)_2Pb_3I_{11}$ is reported in Figure 3a together with the Tauc Plot (inset) from which an optical gap of 1.96 eV (632 nm) is estimated. The emission properties are characterized by a sharp PL peak with maximum at 735 nm, whose excitation profile well corresponds to the absorption (Figure 3b). The PL band displays a FWHM of 130 meV and is characterized by an average lifetime of τ = 2.96 ns, obtained by a three-exponential fit of the decay (see the inset of Figure 3b). The large energy separation between the absorption onset and the PL peak is likely related to emission from layer edge states, located at the crystal edges, after migration of the photogenerated excitons toward lower energy states, as already reported for 2D Ruddlesden−Popper phases with different n values.[83,84]

Electronic Structure. Electronic properties of the newly synthesized $(FA)_3(HEA)_2Pb_3I_{11}$ halide perovskite are elucidated via DFT simulations. These are performed as for the case of the NMR/NQR calculations, relying on the model structure retrieved from XRD measurements at 280 K, so to stay close to the conditions probed experimentally, hence accounting for the role of thermal effects on structural details like the

https://doi.org/10.1021/acs.chemmater.2c00130
Chem. Mater. XXXX, XXX, XXX−XXX

octahedral rotations. In addition, to better clarify the role of the organic spacer in the frontier electronic levels of the material and to avoid spurious effects due to the more difficult resolution of the position of the organic atoms via XRD, we computed the band structure both for model where (i) the organic moieties are substituted by Cs ions and (ii) the positions of the organic atoms are relaxed at zero K (with the inorganic lattice frozen at 280 K). In light of the important role of relativistic effects in the presence of a heavy lead element,[53] DFT electronic structure calculations are carried out including SOC. The resulting band structure shows direct band gap at the D point of the Brillouin zone (Figure 4a,b). The shift of the valence band/conduction band (VB/CB) edges from Γ reflect the presence of only one PbI_6 octahedron per unit cell along the b-crystallographic axis, which does not allow to fold back the antibonding I(p)−Pb(s) and I(s)−Pb(p) hybridization pattern (Figure 4c), peculiar of the frontier orbitals of metal-halide perovskites, at the center of the Brillouin zone.[85] The DFT-SOC single-particle band gap is estimated to be ∼1 eV. Still, one should refrain to compare this with the optical absorption edge, because of the well-known tendency of standard GGA calculations to underestimate the single-particle band gaps[86] and of the very likely presence of excitonic effects in these dimensionally confined systems, as induced by confinement effects,[19] which further stabilize the optical band gap, compared to direct single-particle band-to-band transition. Additional calculations are performed by relaxing all the atomic positions in the crystalline cell (both organic and inorganic), so to roughly estimate the potential impact of structural modifications induced by temperature. The resulting band structure in the Supporting Information (Figure S11) clearly shows that thermal effects do impact the electronic properties but only to a minor extent, for example, band gap opens by ∼60 meV. Interestingly, a small displacement of the conduction band minimum from the high symmetry point D is found, which may be ascribed to the Rashba effect, as induced by structural distortion.[87]

As for the case of <1 0 0>-oriented hybrid perovskites build from nonconjugated cations,[19] the organic component does not contribute to the frontier orbitals of $(FA)_3(HEA)_2Pb_3I_{11}$. This clearly emerges when comparing the results of the calculations performed in the presence of the specific FA and HEA molecules and of the Cs atoms at their place, showing almost equivalent band dispersion along the $C \rightarrow Z \rightarrow D \rightarrow E_0$ path. Most notably, small but non-negligible dispersion is found along the $D \rightarrow Z$ direction in Figure 4a, both for the valence and conduction band edges, hence indicating that consecutive layers are not fully decoupled but they maintain the electronic communication. This is very important from an application viewpoint, as the weak interplanar electronic communication and reduced charge transport along the plane stacking direction are usually considered some of the main culprits for the lower efficiencies of layered perovskite-based optoelectronic devices, compared to those constituted by their 3D analogues.[37,88,89] In the case of the $(FA)_3(HEA)_2Pb_3I_{11}$ layered perovskite, our band structure calculations indicate 36 meV/41 meV band dispersion along the $D \rightarrow Z$ direction for the valence and conduction band edges (Figure 4d), respectively. Corresponding hole and electron effective masses are estimated here to be 1.26 and 1.07 m_e (see Table 2), respectively, which are surprisingly small for disconnected PbI_6 octahedra and which are likely related to the short I...I interlayer distance of 4.55 Å (vide infra and Figure 4d). For the sake of reference, flat band dispersion and infinite hole and electron effective masses were found in the literature for the monoclinic and orthorhombic phases of hexylammonium lead iodide, in correspondence with significantly larger I...I interlayer distances (ca. 8.35 Å).[90,91] In this sense, the larger band dispersion/smaller effective masses in correspondence of shorted interlayer distance are fully expected, as this allows for more effective hybridization of the atomic orbitals. One may therefore wonder whether the specific <1 1 0> termination can have an impact on the interlayer electronic communication.[92] To address this point, we have performed additional calculations on the (4AMP)-$(MA)_2Pb_3I_{10}$ layered perovskite, an analogue with <1 0 0> termination with thickness of the inorganic frame of three octahedra (n = 3), reported in the recent literature.[48,64] The corresponding I...I distance is even shorter for this n = 3 $(4AMP)(MA)_2Pb_3I_{10}$ layered perovskite when compared to the m = 3 $(FA)_3(HEA)_2Pb_3I_{11}$ structure, with correspondingly increasing band dispersion along the stacking direction (see Figure 4d) and reduced hole and electron effective masses of 0.35 and 0.35, respectively. In this sense, the reduced effective mass when going from m = 3 to n = 3 is ascribable both to the shorter I...I distance and to the absence of shift between subsequent perovskite layers (eclipsed configuration).

Table 2. Diagonal Component of the Effective Mass Tensor for Hole (m_h) and Electron (m_e) Carriers, Computed for the Newly Reported $(FA)_3(HEA)_2Pb_3I_{11}$ <1 1 0>-Oriented Layered Perovskites and for $(4AMP)(MA)_2Pb_3I_{10}$, as the Reference for <1 0 0>-Oriented Layered Perovskite with a Comparable Pb/I Ratio[a]

	$(FA)_3(HEA)_2Pb_3I_{11}$ (m = 3)	$(4AMP)(MA)_2Pb_3I_{10}$ (n = 3)
out-of-plane		
m_h	1.26	0.35
m_e	1.07	0.35
in-plane		
m_h	0.17	0.17
m_e	0.11	0.14

[a]Effective masses are evaluated from band dispersion along the crystallographic direction corresponding to the $Pb-I_{equatorial}-Pb$ bonds (in-plane) and along the plane stacking direction (out-of-plane).

To further assess the potential of $(FA)_3(HEA)_2Pb_3I_{11}$ for optoelectronic applications that require attractive carrier transport properties, we computed in-plane effective masses. From the band edge dispersion with respect to the crystallographic direction corresponding to the $Pb-I_{equatorial}-Pb$ bond, we found hole effective masses of ca. 0.17 m_h both for $(FA)_3(HEA)_2Pb_3I_{11}$ and for $(4AMP)(MA)_2Pb_3I_{10}$ layered perovskites, that is, slightly smaller than corresponding masses in n = 1 hexylammonium and dodecylammonium halide perovskites.[90] In-plane electron effective masses m_e are also small both for $(FA)_3(HEA)_2Pb_3I_{11}$ and $(4AMP)(MA)_2Pb_3I_{10}$ (see Table 2), with a slightly smaller value for the former likely due to the almost linear Pb−I−Pb bonds, as retrieved from XRD measurements (vide infra). Effective masses from Table 2 overall suggest the suitability of the present <1 1 0>-oriented perovskites as active materials for optoelectronic devices.

CONCLUSIONS

Combining the excellent semiconducting properties of halide perovskite frames together with improved chemical resistance

https://doi.org/10.1021/acs.chemmater.2c00130
Chem. Mater. XXXX, XXX, XXX−XXX

against moisture, layered halide perovskites have great potential for efficient and stable optoelectronic devices. Multilayered compounds, for which the 2D perovskite network is not confined to only one octahedron thickness but spans over several octahedra, are of particular interest, with the <1 0 0>-oriented family currently widely investigated. On the other hand, also <1 1 0>-oriented layered perovskites can be designed, whose properties have been much less explored, thus far. Here, a new member of the multilayered corrugated <1 1 0>-oriented hybrid metal-halide perovskite, $(FA)_3(HEA)_2Pb_3I_{11}$, has been synthesized and characterized. In particular, by combining X-ray diffraction on crystals and NMR on powders, we successfully resolved its structure, which represents the only crystalline model for multilayered <1 1 0>-oriented compounds reported so far. The newly reported compound shows optical absorption edge around 2 eV and in-plane effective masses comparable to those of (4AMP)-$(MA)_2Pb_3I_{10}$ <1 0 0>-oriented layered perovskite, which was successfully exploited as a photoactive material in photovoltaic devices.[48] The overall picture is hence that <1 1 0>-oriented multilayered halide perovskites may be successfully used in technological fields where <1 0 0>-analogues are currently under scrutiny. In particular, $(FA)_3(HEA)_2Pb_3I_{11}$ has small effective masses along the plane stacking direction, as a result of short distance between iodine atoms belonging to consecutive inorganic sheets, hence imparting more isotropic transport properties to this natively structurally confined material. Unfortunately, this new $m = 3$ member faces stability issues under pressure and humidity, although its stability against moisture is improved compared to $MAPbI_3$. All these findings pave the path toward new efforts to design/synthesize novel high m-value members with increased stability and improved carrier mobilities, namely with eclipsed interlayer packing.

■ ASSOCIATED CONTENT

Supporting Information

The Supporting Information is available free of charge at https://pubs.acs.org/doi/10.1021/acs.chemmater.2c00130.

Experimental details for synthesis, additional structural, NMR, and calorimetry data (PDF)

■ AUTHOR INFORMATION

Corresponding Authors

Nicolas Mercier − *MOLTECH-Anjou, UMR-CNRS 6200, Université d'Angers, 49045 Angers, France;* orcid.org/0000-0003-0458-0789; Email: nicolas.mercier@univ-angers.fr

Claudine Katan − *Univ. Rennes, ENSCR, INSA Rennes, CNRS, ISCR (Institut des Sciences Chimiques de Rennes), UMR 6226, Rennes F-35000, France;* orcid.org/0000-0002-2017-5823; Email: claudine.katan@univ-rennes1.fr

Authors

Maroua Ben Haj Salah − *MOLTECH-Anjou, UMR-CNRS 6200, Université d'Angers, 49045 Angers, France*

Magali Allain − *MOLTECH-Anjou, UMR-CNRS 6200, Université d'Angers, 49045 Angers, France*

Antonin Leblanc − *MOLTECH-Anjou, UMR-CNRS 6200, Université d'Angers, 49045 Angers, France*

Jens Dittmer − *Institut des Molécules et des Matériaux du Mans, CNRS UMR 6283, Le Mans Université, 72085 Le Mans Cedex 9, France*

Chiara Botta − *Istituto di Scienze e Tecnologie Chimiche "G. Natta" (SCITEC), CNR, 20133 Milano, Italy;* orcid.org/0000-0001-8722-0417

Claudio Quarti − *Univ. Rennes, ENSCR, INSA Rennes, CNRS, ISCR (Institut des Sciences Chimiques de Rennes), UMR 6226, Rennes F-35000, France; Laboratory for Chemistry of Novel Materials, University of Mons, B-7000 Mons, Belgium;* orcid.org/0000-0002-5488-1216

Complete contact information is available at: https://pubs.acs.org/10.1021/acs.chemmater.2c00130

Author Contributions

The manuscript was written through contributions of all authors. All authors have given approval to the final version of the manuscript.

Notes

The authors declare no competing financial interest.

■ ACKNOWLEDGMENTS

At ISCR and MOLTECH-Anjou the work was mainly supported by the Agence Nationale pour la Recherche (MORELESS project). For DFT calculations, this work was granted access to the HPC resources of TGCC/CINES/IDRIS under the allocation 2020-A0090907682 made by GENCI. C.Q. is an FNRS research associate.

■ REFERENCES

(1) Mitzi, D. B. *Progress in Inorganic Chemistry*; Karlin, K. D., Ed.; John Wiley & Sons, Inc.: Hoboken, NJ, USA, 1999; pp 1−121

(2) Mitzi, D. B.; Feild, C. A.; Harrison, W. T. A.; Guloy, A. M. Conducting Tin Halides with a Layered Organic-Based Perovskite Structure. *Nature* **1994**, *369*, 467−469.

(3) Mitzi, D. B.; Wang, S.; Feild, C. A.; Chess, C. A.; Guloy, A. M. Conducting Layered Organic-inorganic Halides Containing ⟨110⟩-Oriented Perovskite Sheets. *Science* **1995**, *267*, 1473−1476.

(4) Kagan, C. R.; Mitzi, D. B.; Dimitrakopoulos, C. D. Organic-Inorganic Hybrid Materials as Semiconducting Channels in Thin-Film Field-Effect Transistors. *Science* **1999**, *286*, 945−947.

(5) Mitzi, D. B. Templating and Structural Engineering in Organic-Inorganic Perovskites. *J. Chem. Soc., Dalton Trans.* **2001**, 1−12.

(6) Calabrese, J.; Jones, N. L.; Harlow, R. L.; Herron, N.; Thorn, D. L.; Wang, Y. Preparation and Characterization of Layered Lead Halide Compounds. *J. Am. Chem. Soc.* **1991**, *113*, 2328−2330.

(7) Ishihara, T.; Takahashi, J.; Goto, T. Exciton State in Two-Dimensional Perovskite Semiconductor $(C_{10}H_{21}NH_3)_2PbI_4$. *Solid State Commun.* **1989**, *69*, 933−936.

(8) Era, M.; Morimoto, S.; Tsutsui, T.; Saito, S. Organic-inorganic heterostructure electroluminescent device using a layered perovskite semiconductor $(C_6H_5C_2H_4NH_3)_2PbI_4$. *Appl. Phys. Lett.* **1994**, *65*, 676−678.

(9) Papavassiliou, G. C. Three- and Low-Dimensional Inorganic Semiconductors. *Prog. Solid State Chem.* **1997**, *25*, 125−270.

(10) Mercier, N.; Poiroux, S.; Riou, A.; Batail, P. Unique Hydrogen Bonding Correlating with a Reduced Band Gap and Phase Transition in the Hybrid Perovskites $(HO(CH_2)_2NH_3)_2PbX_4$ (X = I, Br). *Inorg. Chem.* **2004**, *43*, 8361−8366.

(11) Lemmerer, A.; Billing, D. G. Lead halide inorganic−organic hybrids incorporating diammonium cations. *CrystEngComm* **2012**, *14*, 1954−1966.

(12) Shao, S.; Loi, M. A. Advances and Prospective in Metal Halide Ruddlesen−Popper Perovskite Solar Cells. *Adv. Energy Mater.* **2021**, *11*, No. 2003907.

(13) Zhang, F.; Lu, H.; Tong, J.; Berry, J. J.; Beard, M. C.; Zhu, K. Advances in Two-Dimensional Organic-Inorganic Hybrid Perovskites. *Energy Environ. Sci.* **2020**, *13*, 1154−1186.
(14) Grancini, G.; Nazeeruddin, M. K. Dimensional Tailoring of Hybrid Perovskites for Photovoltaics. *Nat. Rev. Mater.* **2019**, *4*, 4−22.
(15) Mao, L.; Stoumpos, C. C.; Kanatzidis, M. G. Two-Dimensional Hybrid Halide Perovskites: Principles and Promises. *J. Am. Chem. Soc.* **2019**, *141*, 1171−1190.
(16) Smith, M. D.; Connor, B. A.; Karunadasa, H. I. Tuning the Luminescence of Layered Halide Perovskites. *Chem. Rev.* **2019**, *119*, 3104−3139.
(17) Li, X.; Hoffman, J. M.; Kanatzidis, M. G. The 2D Halide Perovskite Rulebook: How the Spacer Influences Everything from the Structure to Optoelectronic Device Efficiency. *Chem. Rev.* **2021**, *121*, 2230−2291.
(18) Saparov, B.; Mitzi, D. B. Organic-Inorganic Perovskites: Structural Versatility for Functional Materials Design. *Chem. Rev.* **2016**, *116*, 4558−4596.
(19) Katan, C.; Mercier, N.; Even, J. Quantum and Dielectric Confinement Effects in Lower-Dimensional Hybrid Perovskite Semiconductors. *Chem. Rev.* **2019**, *119*, 3140−3192.
(20) Kojima, A.; Teshima, K.; Shirai, Y.; Miyasaka, T. Organometal Halide Perovskites as Visible-Light Sensitizers for Photovoltaic Cells. *J. Am. Chem. Soc.* **2009**, *131*, 6050−6051.
(21) Turren-Cruz, S.-H.; Hagfeldt, A.; Saliba, M. Methylammonium-Free, High-Performance and Stable Perovskite Solar Cells on a Planar Architecture. *Science* **2018**, *362*, 449−453.
(22) Gratzel, M. The Rise of Highly Efficient and Stable Perovskite Solar Cells. *Acc. Chem. Res.* **2017**, *50*, 487−491.
(23) Jena, A. K.; Kulkarni, A.; Miyasaka, T. Halide Perovskite Photovoltaics: Background, Status, and Future Prospects. *Chem. Rev.* **2019**, *119*, 3036−3103.
(24) Snaith, H. J. Present status and future prospects of perovskite photovoltaics. *Nat. Mater.* **2018**, *17*, 372−376.
(25) Aristidou, N.; Eames, C.; Islam, M. S.; Haque, S. A. Insights into the Increased Degradation Rate of $CH_3NH_3PbI_3$ Solar Cells in Combined Water and O_2 Environments. *J. Mater. Chem. A* **2017**, *5*, 25469−25475.
(26) Manser, S.; Saidaminov, M. I.; Christians, J. A.; Bakr, O. M.; Kamat, P. V. Making and Breaking of Lead Halide Perovskites. *Acc. Chem. Res.* **2016**, *49*, 330−338.
(27) Kaezmi, M. A. A.; Raval, P.; Cherednichekno, K.; Chotard, J.-N.; Krishna, A.; Demortiere, A.; Reddy, G. N. M.; Sauvage, F. Molecular-Level Insight into Correlation between Surface Defects and Stability of Methylammonium Lead Halide Perovskite Under Controlled Humidity. *Small Methods* **2021**, *5*, No. 2000834.
(28) Dohner, E. R.; Hoke, E. T.; Karunadasa, H. I. Self-Assembly of Broadband White-Light Emitters. *J. Am. Chem. Soc.* **2014**, *136*, 1718−1721.
(29) Dohner, E. R.; Jaffe, A.; Bradshaw, L. R.; Karunadasa, H. I. Intrinsic White-Light Emission from Layered Hybrid Perovskites. *J. Am. Chem. Soc.* **2014**, *136*, 13154−13157.
(30) Smith, M. D.; Karunadasa, H. I. White-Light Emission from Layered Halide Perovskites. *Acc. Chem. Res.* **2018**, *51*, 619−627.
(31) Booker, E. P.; Thomas, T. H.; Quarti, C.; Stanton, M. R.; Dashwood, C. D.; Gillett, A. J.; Richter, J. M.; Pearson, A. J.; Davis, N. J. L. K.; Sirringhaus, H.; Price, M. B.; Greenham, N. C.; Beljonne, D.; Dutton, S. E.; Deschler, F. Formation of Long-Lived Color Centers for Broadband Visible Light Emission in Low-Dimensional Layered Perovskites. *J. Am. Chem. Soc.* **2017**, *139*, 18632−18639.
(32) Liu, X.-K.; Gao, F. J. Organic−Inorganic Hybrid Ruddlesden−Popper Perovskites: An Emerging Paradigm for High-Performance Light-Emitting Diodes. *J. Phys. Chem. Lett.* **2018**, *9*, 2251−2258.
(33) Wang, N.; Cheng, L.; Ge, R.; Zhang, S.; Miao, Y.; Zou, W.; Yi, C.; Sun, Y.; Cao, Y.; Yang, R.; Wei, Y.; Guo, Q.; Ke, Y.; Yu, M.; Jin, Y.; Liu, Y.; Ding, Q.; Di, D.; Yang, L.; Xing, G.; Tian, H.; Jin, C.; Gao, F.; Friend, R. H.; Wang, J.; Huang, W. Perovskite light-emitting diodes based on solution-processed self-organized multiple quantum wells. *Nat. Photonics* **2016**, *10*, 699−704.
(34) Yang, X.; Zhang, X.; Deng, J.; Chu, Z.; Jiang, Q.; Meng, J.; Wang, P.; Zhang, L.; Yin, Z.; You, J. Efficient green light-emitting diodes based on quasi-two-dimensional composition and phase engineered perovskite with surface passivation. *Nat. Commun.* **2018**, *9*, 570−577.
(35) Mercier, N. Hybrid Halide Perovskites: Discussions on Terminology and Materials. *Angew. Chem., Int. Ed.* **2019**, *58*, 17912−17917.
(36) Smith, I. C.; Hoke, E. T.; Solis-Ibarra, D.; McGehee, M. D.; Karunadasa, H. I. A Layered Hybrid Perovskite Solar-Cell Absorber with Enhanced Moisture Stability. *Angew. Chem., Int. Ed.* **2014**, *536*, 312−316.
(37) Tsai, H.; Nie, W.; Blancon, J. C.; Stoumpos, C. C.; Asadpour, R.; Harutyunyan, B.; Neukirch, A. J.; Verduzco, R.; Crochet, J. J.; Tretiak, S.; Pedesseau, L.; Even, J.; Alam, M. A.; Gupta, G.; Lou, J.; Ajayan, P. M.; Bedzyk, M. J.; Kanatzidis, M. G. High-efficiency two-dimensional Ruddlesden-Popper perovskite solar cells. *Nature* **2016**, *536*, 312−316.
(38) Szafranski, M.; Katrusiak, A. Phase Transitions in the Layered Structure of Diguanidinium Tetraiodoplumbate. *Phys. Rev. B* **2000**, *61*, 1026−1035.
(39) Stoumpos, C. C.; Mao, L.; Malliakas, C. D.; Kanatzidis, M. G. Structure−Band Gap Relationships in Hexagonal Polytypes and Low-Dimensional Structures of Hybrid Tin Iodide Perovskites. *Inorg. Chem.* **2017**, *56*, 56−73.
(40) Guo, Y.-Y.; Yang, L.-J.; Biberger, S.; McNulty, J. A.; Li, T.; Schotz, K.; Panzer, F.; Lightfoot, P. Structural Diversity in Layered Hybrid Perovskites, A_2PbBr_4 or $AA'PbBr_4$, Templated by Small Disc-Shaped Amines. *Inorg. Chem.* **2020**, *59*, 12858−12866.
(41) Li, Y.; Zheng, G.; Lin, J. Synthesis, Structure, and Optical Properties of a Contorted-Oriented Layered Hybrid Perovskite: $C_3H_{11}SN_3PbBr_4$. *Eur. J. Inorg. Chem.* **2008**, *2008*, 1689−1692.
(42) Li, Y. Y.; Lin, C. K.; Zheng, G. L.; Cheng, Z. Y.; You, H.; Wang, W. D.; Lin, J. Novel ⟨110⟩-Oriented Organic−Inorganic Perovskite Compound Stabilized by N-(3-Aminopropyl)Imidazole with Improved Optical Properties. *Chem. Mater.* **2006**, *18*, 3463−3469.
(43) Mao, L.; Guo, P.; Kepenekian, M.; Hadar, I.; Katan, C.; Even, J.; Schaller, R. D.; Stoumpos, C. C.; Kanatzidis, M. G. Structural Diversity in White-Light-Emitting Hybrid Lead Bromide Perovskites. *J. Am. Chem. Soc.* **2018**, *140*, 13078−13088.
(44) Guo, Y.-Y.; McNulty, J. A.; Mica, N. A.; Samuel, I. D. W.; Slawin, A. M. Z.; Buhl, M.; Lightfoot, P. Structure-Directing Effects in (110)-Layered Hybrid Perovskites Containing Two Distinct Organic Moieties. *Chem. Commun.* **2019**, *55*, 9935−9938.
(45) Salah, M. B. H.; Mercier, N.; Allain, M.; Zouari, N.; Giovanella, U.; Botta, C. Mechanochromic and Electroluminescence Properties of a Layered Hybrid Perovskite Belonging to the ⟨110⟩ Series. *Eur. J. Inorg. Chem.* **2019**, *2019*, 4527−4531.
(46) McNulty, J. A.; Lightfoot, P. Unprecedented Tin Iodide Perovskite-Like Structures Featuring Ordering of Organic Moieties. *Chem. Commun.* **2020**, *56*, 4543−4546.
(47) Li, X.; Guo, P.; Kepenekian, M.; Hadar, I.; Katan, C.; Even, J.; Stoumpos, C. C.; Schaller, R. D.; Kanatzidis, M. G. Small Cyclic Diammonium Cation Templated (110)-Oriented 2D Halide (X = I, Br, Cl) Perovskites with White-Light Emission. *Chem. Mater.* **2019**, *31*, 3582−3590.
(48) Li, W.; Sidhik, S.; Traore, B.; Asadpour, R.; Hou, J.; Zhang, H.; Fehr, A.; Essman, J.; Wang, Y.; Hoffman, J. M.; Spanopoulos, I.; Crochet, J. J.; Tsai, E.; Strzalka, J.; Katan, C.; Alam, M. A.; Kanatzidis, M. G.; Even, J.; Blancon, J. C.; Mohite, A. D. Light-activated interlayer contraction in two-dimensional perovskites for high-efficiency solar cells. *Nat. Nanotechnol.* **2022**, *17*, 45−52.
(49) Giannozzi, P.; Baroni, S.; Bonini, N.; Calandra, M.; Car, R.; Cavazzoni, C.; Ceresoli, D.; Chiarotti, G. L.; Coccioni, M.; Dabo, I.; Dal Corso, A.; de Gironcoli, S.; Fabris, S.; Fratesi, G.; Gebauer, R.; Gerstmann, U.; Gougoussis, C.; Kokalj, A.; Lazzeri, M.; Martin-Samos, L.; Marzari, N.; Mauri, F.; Mazzarello, R.; Paolini, S.; Pasquarello, A.; Paulatto, L.; Sbraccia, C.; Scandolo, S.; Sclauzero, G.; Seitsonen, A. P.; Smogunov, A.; Umari, P.; Wentzcovitch, R. M.

https://doi.org/10.1021/acs.chemmater.2c00130
Chem. Mater. XXXX, XXX, XXX−XXX

QUANTUM ESPRESSO: a Modular and Open-Source Software Project for Quantum Simulations of Materials. *J. Phys.: Condens. Matter* **2009**, *21*, No. 395502.
(50) van Setten, M. J.; Giantomassi, M.; Bousquet, E.; Verstraete, M. J.; Hamann, D. R.; Gonze, X.; Rignanese, G.-M. The PseudoDojo: Training and grading a 85 element optimized norm-conserving pseudopotential table. *Comput. Phys. Commun.* **2018**, *226*, 39−54.
(51) Quarti, C.; Mosconi, E.; De Angelis, P. Interplay of Orientational Order and Electronic Structure in Methylammonium Lead Iodide: Implications for Solar Cell Operation. *Chem. Mater.* **2014**, *26*, 6557−6569.
(52) Perdew, J. P.; Burke, K.; Ernzerhof, M. Generalized Gradient Approximation Made Simple. *Phys. Rev. B: Condens. Matter Mater. Phys.* **1996**, *77*, 3865−3868.
(53) Even, J.; Pedesseau, L.; Jancu, J.-M.; Katan, C. Importance of Spin−Orbit Coupling in Hybrid Organic/Inorganic Perovskites for Photovoltaic Applications. *J. Phys. Chem. Lett.* **2013**, *4*, 2999−3005.
(54) Monkhorst, H. J.; Pack, J. D. Special Points for Brillouin-Zone Integrations. *Phys. Rev. B: Solid State* **1976**, *13*, 5188−5192.
(55) Grimme, S. Semiempirical GGA-type density functional constructed with a long-range dispersion correction. *J. Comput. Chem.* **2006**, *27*, 1787−1799.
(56) Thonhauser, T.; Cooper, V. R.; Li, S.; Puzder, A.; Hyldgaard, P.; Langreth, D. C. Van der Waals density functional: Self-consistent potential and the nature of the van der Waals bond. *Phys. Rev. B* **2007**, *76*, No. 125112.
(57) Clark, S. J.; Segall, M. D.; Pickard, C. J.; Hasnip, P. J.; Probert, M. I. J.; Refson, K.; Payne, M. C. First principles methods using CASTEP. *Z. Kristallogr.* **2005**, *220*, 567−570.
(58) Van de Walle, C.; Blöchl, P. First-principles calculations of hyperfine parameters. *Phys. Rev. B* **1993**, *47*, 4244.
(59) Pickard, C. J.; Mauri, F. All-electron magnetic response with pseudopotentials: NMR chemical shifts. *Phys. Rev. B* **2001**, *63*, No. 245101.
(60) Quarti, Q.; Furet, E.; Katan, C. DFT Simulations as Valuable Tool to Support NMR Characterization of Halide Perovskites: the Case of Pure and Mixed Halide Perovskites. *Helv. Chim. Acta* **2021**, *104*, No. e2000231.
(61) Alkan, F.; Dybowski, C. Chemical-shift tensors of heavy nuclei in network solids: a DFT/ZORA investigation of ^{207}Pb chemical-shift tensors using the bond-valence method. *Phys. Chem. Chem. Phys.* **2015**, *17*, 25014−25026.
(62) Leblanc, A.; Mercier, N.; Allain, M.; Dittmer, J.; Fernandez, V.; Pauporté, T. Lead and iodide deficient $(CH_3NH_3)PbI_3$, d-MAPI: the bridge between 2D and 3D hybrid perovskites. *Angew. Chem., Int. Ed.* **2017**, *56*, 16067−16072.
(63) Leblanc, A.; Mercier, N.; Allain, M.; Dittmer, J.; Pauporté, T.; Fernandez, V.; Boucher, F.; Kepenekian, M.; Katan, C. Enhanced Stability and Band Gap Tuning of α-$[HC(NH_2)_2]PbI_3$ Hybrid Perovskite by Large Cation Integration. *ACS Appl. Mater. Interfaces* **2019**, *11*, 20743−20751.
(64) Mao, L.; Ke, W.; Pedesseau, L.; Wu, Y.; Katan, C.; Even, J.; Wasielewski, M. R.; Stoumpos, C. C.; Kanatzidis, M. G.; Wasielewski, M. R.; Stoumpos, C. C.; Kanatzidis, M. G. Hybrid Dion−Jacobson 2D Lead Iodide Perovskites. *J. Am. Chem. Soc.* **2018**, *140*, 3775−3783.
(65) Myae Myae Soe, C.; Stoumpos, C. C.; Kepenekian, M.; Traoré, B.; Tsai, H.; Nie, W.; Wang, B.; Katan, C.; Seshadri, R.; Mohite, A. D.; Even, J.; Marks, T. B.; Kanatzidis, M. G. New Type of 2D Perovskites with Alternating Cations in the Interlayer Space, $(C(NH_2)_3)$-$(CH_3NH_3)_nPb_nI_{3n+1}$: Structure, Properties, and Photovoltaic Performance. *J. Am. Chem. Soc.* **2017**, *139*, 16297−16309.
(66) Stoumpos, C. C.; Malliakas, C. D.; Kanatzidis, M. G. Semiconducting Tin and Lead Iodide Perovskites with Organic Cations: Phase Transitions, High Mobilities, and near-Infrared Photoluminescent Properties. *Inorg. Chem.* **2013**, *52*, 9019−9038.
(67) Niu, T.; Xue, Q.; Yip, H.-L. Advances in Dion-Jacobson phase two-dimensional metal halide perovskite solar cells. *Nano* **2021**, *10*, 2069−2102.
(68) Dahlman, C. J.; Kennard, R. M.; Paluch, P.; Venkatesan, N. R.; Chabinyc, M. L.; Reddy, G. N. M. Dynamic Motion of Organic Spacer Cations in Ruddlesden−Popper Lead Iodide Perovskites Probed by Solid-State NMR Spectroscopy. *Chem. Mater.* **2021**, *33*, 642−656.
(69) Dahlman, C. J.; Kubicki, D. J.; Reddy, G. N. Interfaces in metal halide perovskites probed by solid-state NMR spectroscopy. *J. Mater. Chem. A* **2021**, *9*, 19206−19244.
(70) Raval, P.; Kennard, R. M.; Vasileiadou, E. S.; Dahlman, C. J.; Spanopoulos, I.; Chabinyc, M. L.; Kanatzidis, M.; Reddy, G. N. M. Understanding Instability in Formamidinium Lead Halide Perovskites: Kinetics of Transformative Reactions at Grain and Subgrain Boundaries. *ACS Energy Lett.* **2022**, *7*, 1537−1543.
(71) Roiland, C.; Trippé-Allard, G.; Jemli, K.; Alonso, B.; Ameline, J.-C.; Gautier, R.; Bataille, T.; Le Pollès, L.; Deleporte, E.; Even, J.; Katan, C. Multinuclear NMR as a tool for studying local order and dynamics in $CH_3NH_3PbX_3$ (X = Cl, Br, I) hybrid perovskites. *Phys. Chem. Chem. Phys.* **2016**, *18*, 27133−27142.
(72) Kubicki, D. J.; Prochowicz, D.; Hofstetter, A.; Péchy, P.; Zakeeruddin, S. M.; Grätzel, M.; Emsley, L. Dynamics in Mixed-Cation $(MA)_x(FA)_{1-x}PbI_3$ Hybrid Perovskites from Solid-State NMR. *J. Am. Chem. Soc.* **2017**, *139*, 10055−10061.
(73) Van Gompel, W. T. M.; Herckens, R.; Reekmans, G.; Ruttens, B.; D'Haen, J.; Adriaensens, P.; Lutsen, L.; Vanderzande, D. Degradation of the Formamidinium Cation and the Quantification of the Formamidinium−Methylammonium Ratio in Lead Iodide Hybrid Perovskites by Nuclear Magnetic Resonance Spectroscopy. *J. Phys. Chem. C* **2018**, *122*, 4117−4124.
(74) Sharma, S.; Weiden, N.; Weiss, A. Phase transition in $CsSnCl_3$ and $CsPbBr_3$ and NMR and NQR study. *Z. Naturforsch. A* **1991**, *46*, 329−336.
(75) Xu, Q.; Eguchi, T.; Nakayama, H.; Nakamura, N.; Kishita, M. Molecular Motions and Phase Transitions in Solid $CH_3NH_3PbX_3$ (X = C1, Br, I) as Studied by NMR and NQR. *Z. Naturforsch. A* **1991**, *46*, 240−246.
(76) Senocrate, A.; Moudrakovski, I.; Maier, J. Short-range ion dynamics in methylammonium lead iodide by multinuclear solid state NMR and ^{127}I NQR. *Chem. Phys. Phys. Chem.* **2018**, *20*, 20043−20055.
(77) Franssen, W. M. J.; van Es, S. G. D.; Dervişoğlu, R.; de Wijs, G. A.; Kentgens, A. P. M. Symmetry, Dynamics, and Defects in Methylammonium Lead Halide Perovskites. *J. Phys. Chem. Lett.* **2017**, *8*, 61−66.
(78) Piveteau, L.; Morad, V.; Kovalenko, M. V. Solid-State NMR and NQR Spectroscopy of Lead-Halide Perovskite Materials. *J. Am. Chem. Soc.* **2020**, *142*, 19413−19437.
(79) Piveteau, L.; Aebli, M.; Yazdani, N.; Millen, M.; Korosec, L.; Krieg, F.; Benin, B. M.; Morad, V.; Piveteau, C.; Shiroka, T.; Comas-Vives, A.; Coperet, C.; Lindenberg, A. M.; Wood, V.; Verel, R.; Kovalenko, M. V. Bulk and Nanocrystalline Cesium Lead-Halide Perovskites as Seen by Halide Magnetic Resonance. *ACS Cent. Sci.* **2020**, *6*, 1138−1149.
(80) Aebli, M.; Porenta, N.; Aregger, N.; Kovalenko, M. V. Local Structure of Multinary Hybrid Lead Halide Perovskites Investigated by Nuclear Quadrupole Resonance Spectroscopy. *Chem. Mater.* **2021**, *33*, 6965−6973.
(81) Mozur, E. M.; Hope, M. A.; Trowbridge, J. C.; Halat, D. M.; Daemen, L. L.; Maughan, A. E.; Prisk, T. R.; Grey, C. P.; Neilson, J. R. Cesium Substitution Disrupts Concerted Cation Dynamics in Formamidinium Hybrid Perovskites. *Chem. Mater.* **2020**, *32*, 6266−6277.
(82) Sutton, R. J.; Filip, M. R.; Haghighirad, A. A.; Sakai, N.; Wenger, B.; Giustino, F.; Snaith, H. J. Cubic or Orthorhombic? Revealing the Crystal Structure of Metastable Black-Phase $CsPbI_3$ by Theory and Experiment. *ACS Energy Lett.* **2018**, *3*, 1787−1794.
(83) Blancon, J. C.; Tsai, H.; Nie, W.; Stoumpos, C. C.; Pedesseau, L.; Katan, C.; Kepenekian, M.; Soe, C. M. M.; Appavoo, K.; Sfeir, M. Y.; Tretiak, S.; Ajayan, P. M.; Kanatzidis, M. G.; Even, J.; Crochet, J. J.; Mohite, A. D. Extremely efficient internal exciton dissociation

https://doi.org/10.1021/acs.chemmater.2c00130
Chem. Mater. XXXX, XXX, XXX−XXX

through edge states in layered 2D perovskites. *Science* **2017**, *355*, 1288−1292.
(84) Shang, Q.; Wang, Y.; Zhong, Y.; Mi, Y.; Qin, L.; Zhao, Y.; Qiu, X.; Liu, X.; Zhang, Q. Unveiling Structurally Engineered Carrier Dynamics in Hybrid Quasi-Two-Dimensional Perovskite Thin Films toward Controllable Emission. *J. Phys. Chem. Lett.* **2017**, *8*, 4431−4438.
(85) Quarti, C.; Katan, C.; Even, J. Physical properties of bulk, defective, 2D and 0D metal halide perovskite semiconductors from a symmetry perspective. *J. Phys: Mater.* **2020**, *3*, No. 042001.
(86) van Schilfgaarde, M.; Kotani, T.; Faleev, S. Quasiparticle Self-Consistent GW Theory. *Phys. Rev. Lett.* **2006**, *96*, No. 226402.
(87) Kepenekian, M.; Robles, R.; Katan, C.; Sapori, D.; Pedesseau, L.; Even, J. Rashba and Dresselhaus Effects in Hybrid Organic−Inorganic Perovskites: From Basics to Devices. *ACS Nano* **2015**, *9*, 11557−11567.
(88) Cao, D. H.; Stoumpos, C. C.; Farha, O. K.; Hupp, J. T.; Kanatzidis, M. G. 2D Homologous Perovskites as Light-Absorbing Materials for Solar Cell Applications. *J. Am. Chem. Soc.* **2015**, *137*, 7843−7850.
(89) Tsai, H.; Nie, W.; Blancon, J. C.; Stoumpos, C. C.; Myae Myae Soe, C.; Yoo, J.; Crochet, J.; Tretiak, S.; Even, J.; Sadhanala, A.; Azzellino, G.; Brenes, R.; Ajayan, P. M.; Bulovic, V.; Stranks, S. D.; Friend, R. H.; Kanatzidis, M. G.; Mohite, A. D. Stable Light-Emitting Diodes Using Phase-Pure Ruddlesden−Popper Layered Perovskites. *Adv. Mater.* **2018**, *30*, No. 1704217.
(90) Quarti, C.; Marchal, N.; Beljonne, D. Tuning the Optoelectronic Properties of Two-Dimensional Hybrid Perovskite Semiconductors with Alkyl Chain Spacers. *J. Phys. Chem. Lett.* **2018**, *9*, 3416−3424.
(91) Billing, D. G.; Lemmerer, A. Synthesis, characterization and phase transitions in the inorganic−organic layered perovskite-type hybrids $[(C_nH_{2n+1}NH_3)_2PbI_4]$, n = 4, 5 and 6. *Acta Crystallogr., Sect. B: Struct. Sci.* **2007**, *B63*, 735−747.
(92) Marchal, N.; Mosconi, E.; García-Espejo, G.; Almutairi, T. M.; Quarti, Q.; Beljonne, D.; De Angelis, F. Cation Engineering for Resonant Energy Level Alignment in Two-Dimensional Lead Halide Perovskites. *J. Phys. Chem. Lett.* **2021**, *12*, 2528−2535.

https://doi.org/10.1021/acs.chemmater.2c00130
Chem. Mater. XXXX, XXX, XXX−XXX